Autophagy Inhibition Favors Survival of Rubrospinal Neurons After Spinal Cord Hemisection

Elisa Bisicchia[1] · Laura Latini[1] · Virve Cavallucci[1] · Valeria Sasso[1] · Vanessa Nicolin[2] · Marco Molinari[1] · Marcello D'Amelio[1,3] · Maria Teresa Viscomi[1]

Accepted: 1 August 2016

Abstract Spinal cord injuries (SCIs) are devastating conditions of the central nervous system (CNS) for which there are no restorative therapies. Neuronal death at the primary lesion site and in remote regions that are functionally connected to it is one of the major contributors to neurological deficits following SCI.

Disruption of autophagic flux induces neuronal death in many CNS injuries, but its mechanism and relationship with remote cell death after SCI are unknown. We examined the function and effects of the modulation of autophagy on the fate of axotomized rubrospinal neurons in a rat model of spinal cord dorsal hemisection (SCH) at the cervical level. Following SCH, we observed an accumulation of LC3-positive autophagosomes (APs) in the axotomized neurons 1 and 5 days after injury. Furthermore, this accumulation was not attributed to greater initiation of autophagy but was caused by a decrease in AP clearance, as demonstrated by the build-up of p62, a widely used marker of the induction of autophagy. In axotomized rubrospinal neurons, the disruption of autophagic flux correlated strongly with remote neuronal death and worse functional recovery. Inhibition of AP biogenesis by 3-methyladenine (3-MA) significantly attenuated remote degeneration and improved spontaneous functional recovery, consistent with the detrimental effects of autophagy in remote damage after SCH. Collectively, our results demonstrate that autophagic flux is blocked in axotomized neurons on SCI and that the inhibition of AP formation improves their survival. Thus, autophagy is a promising target for the development of therapeutic interventions in the treatment of SCIs.

Keywords Autophagy · Autophagy flux · Spinal cord injury · Neurodegeneration · Autophagosomes · Remote damage

Elisa Bisicchia and Laura Latini contributed equally to this work.

Marcello D'Amelio and Maria Teresa Viscomi are equal senior authors

✉ Marcello D'Amelio
m.damelio@unicampus.it

✉ Maria Teresa Viscomi
mt.viscomi@hsantalucia.it

[1] Santa Lucia Foundation, I.R.C.C.S, Via del Fosso di Fiorano 64, 00143 Rome, Italy

[2] Clinical Department of Medical, Surgical and Health Science, University of Trieste, Trieste, Italy

[3] Department of Medicine, Unit of Molecular Neurosciences, University Campus-Biomedico, Via Alvaro del Portillo, 21, I-00128 Rome, Italy

Abbreviations

CNS	Central nervous system
SCI	Spinal cord injury
SCH	Spinal cord hemisection
3-MA	3-Methyladenine;
Rapa	Rapamycin
FB	Fast-blue
RN	Red nucleus
LC3	Light chain 3
mTOR	Mammalian target of rapamycin
APs	Autophagosomes
AMPK	Adenosine monophosphate-activated protein kinase
cyt-c	Cytochrome-c
Comp C	Compound C
i.c.v.	Intracerebroventricularly

Introduction

Spinal cord injury is one of the most debilitating central nervous system (CNS) pathologies, creating enormous challenges with regard to rehabilitation. This difficulty has prompted extensive clinical and scientific research to develop therapeutic strategies for spinal cord injury (SCI) patients and improve neurological function in what has been historically deemed an untreatable condition [1, 2]. Significant effort has been devoted toward minimizing secondary damage (e.g., inflammation, excitotoxicity, and apoptosis) and promoting myelin regeneration and scar remodeling at the lesion site [3–6].

In addition to the effects that are related to the primary damage, functional impairments following SCI are attributable to degenerative events that occur in regions that are remote but functionally connected to the site of the primary lesion—i.e., supraspinal structures [7]. These events, which include cell death and structural changes, are significant predictors of outcome [8]. Despite their clinical value in determining one's recovery [7, 8], few therapeutic approaches to counteract remote delayed and progressive degeneration after SCI have been proposed.

Autophagy is a catabolic process that balances cellular protein synthesis and degradation, in which misfolded and aggregated proteins, lipids, and organelles are engulfed by double-membrane vesicles, called autophagosomes (APs), and degraded after fusing to lysosomes [9–11]. With regard to the CNS, low levels of autophagy are required for neuronal maintenance [12]. Conversely, disruption of autophagic machinery frequently results in intracellular accumulation of protein and adult-onset degeneration [13, 14], effecting neurodegenerative disorders, such as Alzheimer, Huntington, and Parkinson diseases [15, 16]. Depending on cell type, environment, and manner of stimulation, autophagy can precede, inhibit, or enhance apoptotic cell death, and both autophagic and necrotic morphologies have been observed in the same cell [17].

Several studies have shown such cytoprotective functions after the induction of autophagy and pharmacological stimulation in models of neurodegenerative disorders and traumatic brain injury [18]. We also recently demonstrated a significant function of the activation of autophagy at remote sites in the early stages after acute focal brain damage [19, 20]. Increasing attention has been directed toward the study of autophagy in acute brain injuries, such as SCI. Although an involvement of autophagy has nearly been demonstrated in several experimental models of SCI [21–25], the molecular mechanism that links remote brain damage to autophagy after SCI has not been examined.

In this study, we determined (i) the temporal profile of the AP biogenesis in damaged rubrospinal neurons after dorsal spinal cord hemisection (SCH) and its relationship with neuronal atrophy and apoptosis in the early stages after injury (1, 3, 5, and 7 days); (ii) the function of autophagy in the survival and atrophy of axotomized rubrospinal neurons and in functional recovery; and (iii) the molecular effectors and signaling cascades that underlie autophagy-mediated neuroprotection and neurodegeneration.

Materials and Methods

Animals and Spinal Cord Hemisection

Adult male Wistar rats (200–250 g) were obtained from Harlan (S. Pietro al Natisone, Udine, Italy) and maintained in our animal facilities on a 12:12-h light:dark cycle, receiving food and water ad libitum. Animals were handled in accordance with the guidelines published in the NIH Guide for the Care and Use of Laboratory Animals, the principles laid out in the Guidelines for the Use of Animals in Neuroscience Research published by the Society for Neuroscience, and European Union guidelines (Council Directive 86/609/EEC). Protocol was approved by the Italian Ministry of Health (Prot. Number: DM444/2015/PR). Special care was taken to use the minimum number of animals required for statistical accuracy. For surgical procedures, the rats were deeply anesthetized by intraperitoneal (i.p.) injections of Rompun (xylazine, 20 mg/ml, 0.5 ml/kg Bayer, Milan, Italy) and Zoletil (tiletamine and zolazepam, 100 mg/ml, 0.5 ml/kg; Virbac, Milan, Italy).

Ten days before lesion animals underwent a right-side C5/C6 intraspinal injection of Fast-blue (FB) to retrogradely label the cervical projecting neurons of the red nucleus (RN) (Fig. 1). For this purpose, hair overlying the cervical vertebrae was removed, the skin was treated with betadine and incised, and the layers of muscle were bluntly dissected. The dura was removed using blunt iridectomy scissors and a fine forceps and a right-side C5/C6 intraspinal injection of 5 μl of 2 % FB (Sigma F5756) was performed. After FB injection, the muscles were sutured in layers and the skin was closed with wound clips. Ten days after, animals underwent spinal cord injury surgery. After anesthesia (as above), the skin was

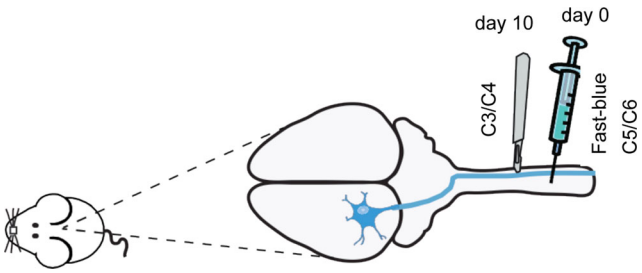

Fig. 1 Schematic of spinal cord hemisection (*SCH*) model employed in the study. Because of the crossed organization of the rubro-spinal tracts, a right cervical hemisection axotomizes virtually all neurons of the contralateral red nucleus (*RN*) that were labeled by a single injection of the retrograde tracer Fast-blue (*FB*) performed at level C5/C6 10 days before spinal cord hemisection at the C3/C4 level

treated with betadine and incised, and the layers of muscle were bluntly dissected. A dorsal unilateral laminectomy was performed at C4 to expose the dura-covered spinal cord. The dura was removed using blunt iridectomy scissors and a fine forceps. Vertebral segment C4 (corresponding to spinal segment C3/C4) was identified by counting of vertebral spines from segment T2. Using sharp iridectomy scissors, a lateral SCH was performed. To ensure the completeness of the injury, a 30-gauge needle was swept through the injury site. Muscle and skin layers were repaired using 5–0 Vicryl sutures and rats were allowed to recover on a heated blanket before being returned to their home cage. Control (CTRL) animals received only a dorsal unilateral laminectomy at C4 to expose the dura-covered spinal cord.

After surgery, animals received an analgesic (2.5 mg per subcutaneous injection of Rimadyl; Pfizer) once per day for 5 days and antibiotics (1.25 mg/250 g body weight intraperitoneal injection of Baytril; Bayer) once per day for 3 days. Animal weights were recorded daily for a week post-surgery, and twice a week thereafter. Bladder function was also assessed for 7 days post-surgery, but every animal retained bladder function post-operatively, and no expressions were necessary. The animals were monitored for hydration and eventual infections until the end of the experiment. SCHs were histologically verified postmortem. Incompletely injured or over-hemisected rats were subsequently eliminated from our study.

Drug Treatment

The following drugs were used: Rapamycin (Rapa; Alexis Biochemicals, BML-A275) was dissolved in DMSO (25 mg/ml) and saline and injected once daily (3 mg/kg; i.p.). 3-Methyladenine (3-MA; Sigma, M2780) was dissolved in DMSO (10 mg/ml) and saline and injected once daily (3 mg/kg; i.p.) for 5 days. Compound C (Comp C; 0.1 μmol; Sigma, P5499) was dissolved in DMSO and saline and injected (10 μl) intracerebroventricularly (i.c.v.) 60 min before lesion; E64d (Sigma, E8640) was dissolved in DMSO (10 mg/ml) and saline and injected once daily (5 mg/kg; i.p.) for 5 days. Furthermore, for each set of experiments, a group of animals were injected with vehicle (saline; 400 μl i.p., once daily for 5 days).

Histology and Immunohistochemistry

Rats were perfused transcardially with 250 ml of saline followed by 250 ml of 4 % paraformaldehyde in a phosphate buffer (PB; 0.1 M; pH .4) under anesthesia induced by i.p. injection of sodium pentobarbital (60 mg/kg). Each brain and spinal cord was removed immediately, post-fixed in the same fixative for 2 h and, after three washes in PB, transferred to 30 % sucrose in PB solution at 4 °C until they sank. Brains and spinal cord were cut into four series of 30-μm-thick transverse sections by means of a freezing microtome and were collected in PB.

To investigate autophagy activation and its relationship with apoptosis in damaged rubrospinal neurons, sections presenting FB-positive neurons were incubated overnight with a cocktail of primary antibodies, including rabbit anti-light chain 3 (LC3) (1:200; Novus Bio, NB100-2220), mouse anti-NeuN (1:200; Millipore, MAB377), and goat anti-cytochrome-c (Santa Cruz Biotechnology, SC-8385). All primary antibody solutions were prepared in PB and 0.3 % Triton X-100 and were incubated 48 h at 4 °C. Each incubation step was followed by three, 5-min rinses in PB. Afterwards, sections were incubated 2 h at RT with a cocktail of secondary antibodies, including Alexa Fluor 647 conjugated donkey anti-mouse (1:200; Invitrogen), Alexa Fluor 543 conjugated donkey anti-rabbit (1:200), and Alexa Fluor 488 conjugated donkey anti-goat (1:200). Sections were examined under a confocal laser scanning microscope (Zeiss LSM700, Germany) equipped with four laser lines: violet diode emitting at 405 nm (for DAPI), argon emitting at 488 nm, and helium/neon emitting at 543 nm and 633 using a ×40/0.5 NA oil objective. Images were exported in TIFF format, contrast and brightness were adjusted, and final plates were composed with Adobe Illustrator CS3 or Corel Draw 9.

Densitometric Analysis of Fluorescence Images

Densitometric analysis of LC3 protein and cytochrome-c (cyt-c) release was performed on perfused rat brain sections. In order to avoid staining variability among sections and experimental groups, sections of rat brains were incubated with the appropriate primary and secondary antibodies at the same time. Furthermore, confocal settings for image capture were maintained constant throughout the acquisition of sections from the experimental groups of rats.

After background subtraction, LC3- and cyt-c-associated signals were quantified by manually outlining individual FB-positive neurons and measuring cell-associated fluorescence intensity with the ImageJ software (http://rsb.info.nih.gov/ij). The F/A ratio defines mean fluorescence of individual cells (F) normalized to total cellular surface (A). Quantification was done on 250 cells per group. Data collecting for densitometry was done by experimenter blind to the group analyzed.

Neuronal Cross-Sectional Area Measurement

For the measurement of neuronal cross-sectional area, Nissl staining was performed on sections presenting Fast blue-positive neurons. Since atrophy of rubrospinal neurons is recognized to make the borders of the axotomized red nucleus (RN) less distinct, Fast-blue retrograde labeling was used as

an anatomical reference for demarcating the magnocellular RN. Quantification of rubrospinal neurons size and cell number was performed using five alternate sections of 30-μm regularly spaced throughout the entire RN rostro-caudal extension. Only neurons identified by a clear nuclear profile were included for analysis. Rubrospinal neurons mean cell area was expressed as percentage of rubrospinal neurons mean cell area of CTRL animals.

Stereological Analyses

To assess the extent of cell loss in RN following SCH, stereological cell count of Fast-blue/Nissl-stained rubrospinal neurons, identified by a clear nuclear profile, was performed. To better appreciate the effects of SCH on rubrospinal neurons loss, we related the number of surviving rubrospinal neurons to the number of neurons present in the RN of unlesioned animals (CTRL).

Quantitative analyses were limited to the RN of the experimental side projecting to the lesioned spinal cord. Using the Stereo Investigator System (MicroBrightField Europe e.K., Magdeburg, Germany), an optical fractionator, stereological design was applied to obtain unbiased estimates of total Nissl-stained and FB-positive neurons. A stack of MAC 5000 controller modules (Ludl Electronic Products, Ltd. Hawthorne, NY, USA) was configured to interface an Olympus BX 50 microscope with a motorized stage and a HV-C20 Hitachi color digital camera with a Pentium II PC workstation. A three-dimensional optical fractionator counting probe (x, y, z dimensions of 50 × 50 × 10 μm, respectively) was applied. The RN was outlined using the ×5 objective, and FB was used as an anatomical reference for demarcating the magnocellular RN, while the ×100 oil immersion objective was used for marking the neuronal cells. The total number of rubrospinal neurons was estimated according to the formula given below:

$$N = \mathrm{SQ} \times 1 / \mathrm{ssf} \times 1 / \mathrm{asf} \times 1 / \mathrm{tsf}$$

where SQ represents the total number of neurons counted in all optically sampled fields of the RN, ssf is the section sampling fraction, asf is the area sampling fraction, and tsf is the thickness sampling fraction.

Mitochondrial and Cytosolic Fraction

Red nuclei were homogenized in buffer A (320 mM sucrose, 1 mM EDTA, 50 mM TRIS-HCl pH .4, 1 mM DTT, 1 mM PMSF), with protease inhibitor cocktail (Sigma, P8340) by 30 strokes with a glass Pyrex micro homogenizer. The homogenate was centrifuged at 1000×g for 10 min, and the resulting supernatant was centrifuged at 10,000×g for 20 min to obtain the mitochondrial pellet and the supernatant. The mitochondria-containing pellet was washed three times with buffer B (250 mM sucrose, 1 mM EGTA–Sigma, E3889, 10 mM TRIS-HCl pH. 4) by centrifugation for 10 min at 10,000×g. The supernatant was centrifuged at 100,000×g for 1 h to generate the cytosolic fraction.

Western Blotting

Red nuclei were homogenized in lysis buffer (320 mM sucrose, 10 % glycerol, 50 mM NaCl, 50 mM TRIS-HCl, pH. 5, 1 % Triton X-100, 1 mM PMSF) with protease inhibitor cocktail (Sigma, P8340), incubated on ice for 30 min and centrifuged at 13,000×g for 20 min. The total protein content of resulting supernatant was determined. Proteins were applied to SDS-PAGE and electroblotted on a PVDF membrane. Immunoblotting analysis was performed using chemiluminescence detection kit. The relative levels of immunoreactivity were determined by densitometry using ImageJ software (NIH; USA). Samples were incubated with the following primary antibodies: mouse anti-cytochrome-c (1:1000; BD Pharmingen, UK); rabbit polyclonal anti-p62 (1:1000; MBL International); mouse monoclonal anti-LC3 (1:250; Nanotools,); mouse monoclonal anti-Becn1 (1:1000; BD Transduction Laboratories); mouse monoclonal anti-cyrochrome-c (1:1000; BD PharMingen); rabbit anti-ULK1 (1:1000; Santa Cruz Biotechnology); mouse anti-p-ULK1 (Ser555) (1:1000; Cell Signaling); rabbit anti-p-ULK1 (Ser757) (1:1000; Cell Signaling); rabbit anti-p-S6 Ribosomal Protein (Ser240/244) (1:1000; Cell Signaling); mouse anti-S6 Ribosomal Protein (1:1000; Cell Signaling); mouse anti-AMPK (1:1000; Cell Signaling); rabbit anti-p-AMPK (1:1000; Cell Signaling); rabbit anti-mTOR (1:1000; Cell Signaling); rabbit anti-p-mTOR (1:1000; Cell Signaling); and mouse anti-GAPDH (1:5000; Abcam, UK). Densities of protein bands in the Western blots were measured, and mean ratios between proteins and GAPDH were reported as percentage of control values.

Beam-Walking Test

Animals were examined with a fine-motor test paradigm (beam-walking test) at 0 and 1, 3, and 5 days after surgery. In the fine-motor behavior test, the locomotion of the rats was evaluated pre-operatively and post-operatively using a beam-walking task with an elevated narrow beam (150 cm long × 2.5 cm wide). The worst score (‘0’) was given if the rat was unable to traverse the beam and could neither place the affected limbs on the horizontal surface nor maintain balance. A score of ‘1’ was given if the rat was unable to traverse the beam or to place the affected limbs on the horizontal surface of the beam but was able to maintain balance. A score of ‘2’ was given if the rat was unable to traverse the beam but placed the affected limbs on the horizontal surface of the beam and maintained balance. A score of ‘3’ was given if the rat used the

affected limbs in less than half of its steps along the beam. A score of '4' was given if the rat traversed the beam and used the affected limbs to aid with more than 50 % of its steps along the beam.

A score of '5' was given if the rat traversed the beam and used the affected limbs to aid with less than 50 % of its steps along the beam. A score of '6' was given if the rat traversed the beam normally with no more than two-foot slips. The week before surgery, animals were trained to run the narrow beam for a food reward once daily, 5 days per week. All the animals in all groups underwent the motor behavior test to ensure that their performance score before surgery (day 0) was 6. An investigator who was blinded to the experimental groups conducted these experiments.

Statistical Analysis

All values were expressed as mean ± S.E.M. when not otherwise specified. Differences between means were analyzed using one-way ANOVA with Bonferroni post hoc test. All statistical analyses were performed using Prism-5 software (GraphPAD Software for Science, USA) with significance set at $P < 0.05$. All quantitative analyses were conducted blind to the animal's experimental groups.

Results

Autophagosomes Accumulate in Axotomized Rubrospinal Neurons After SCH

To examine the induction of autophagy after SCH, we sacrificed the animals at 0, 1, 3, 5, and 7 days after injury, and autophagy in the contralateral red nucleus (RN) was monitored using various approaches accordingly to guidelines for detecting and monitoring autophagy [26, 27].

After SCH, autophagic activity was tracked by changes in the conversion of microtubule-associated protein 1 light chain 3 (LC3) from its nonlipidated (LC3-I) to lipidated form (LC3-II). During autophagy, the conversion of LC3-I to LC3-II is required for APs formation and is detected as a mobility shift by protein gel blot.

In the time course analysis, we noted a time-dependent increase in the levels of LC3-II/LC3-I ratio, suggestive of APs formation, peaking 1 day after injury, remaining high between 3 and 5 days, and then falling slightly (Fig. 2a). Furthermore, quantitative analysis of densitometric values of LC3 immunostaining confirmed a time-dependent increase of LC3 signal in Fast blue-positive rubrospinal neurons after SCH (Fig. 2b). Indeed, as shown in Fig. 2c, SCH induced the formation of active APs, detected as an increase in green

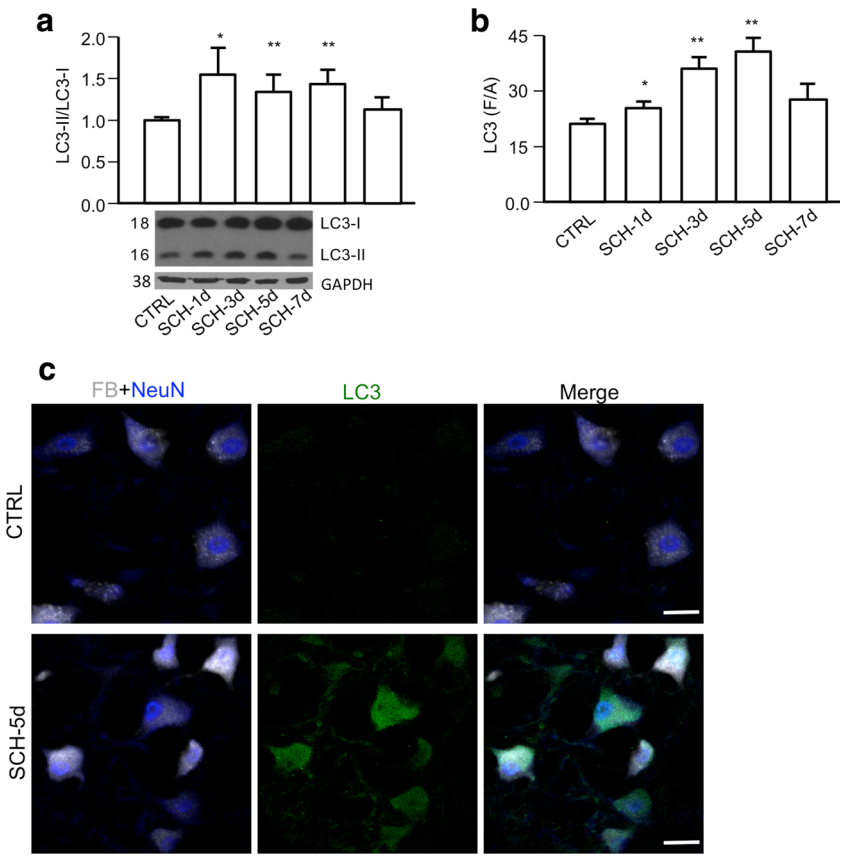

Fig. 2 Spinal cord hemisection modulates key proteins involved in APs formation. **a** LC3 immunoblots and densitometric graphs in controls (*CTRL*) and lesioned (*SCH*) animals at various time points after damage. Note that starting from 1 day until 5 days the LC3-II/LC3-I ratio in *SCH* is increased compared to *CTRL*. Data are expressed as mean ± s.d. ($n = 8$/group). **b** Histograms of densitometric values of LC3 signal, expressed as mean fluorescence of Fast blue-positive neurons (*F*), normalized to total cellular surface (**a**) in CTRL, SCH-1d, SCH-3d, SCH-5d, SCH-7d (F/A; $n = 250$ cells/group). One-way ANOVA followed by Bonferroni multiple comparison test. $*p < 0.05$, $**p < 0.01$ vs. CTRL. **c** Triple-labeled and merged confocal images of NeuN (*blue*) plus Fast blue (*FB*; *gray*) and LC3 (*green*) in red nucleus of *CTRL* and 5 days after *SCH*. *Scale bars* = 25 μm

fluorescence signal (LC3) compared with CTRL animals, suggesting the presence of active APs in damaged rubrospinal neurons (Fig. 2c). Collectively, our biochemical and morphological data demonstrate greater APs formation in rubrospinal neurons after SCH.

To determine the molecular mechanism of autophagy activation after SCH, we measured the levels of ULK1 complex, which mediates the initiation of autophagy [28]. In our time course analysis, p-ULK1$^{(Ser555)}$ levels rose time-dependently in SCH animals compared with controls (Fig. 3a), with similar kinetics as LC3 (Fig. 2a).

Mammalian target of rapamycin (mTOR) and AMP-activated protein kinase (AMPK) directly phosphorylate ULK1 at different sites and coordinate mammalian autophagy [29, 30]. Thus, we examined the signaling pathways that are involved in ULK1 activation by Western blot. The p-AMPK$^{(Thr172)}$/AMPK ratio increased significantly from day 1 and remained elevated until day 7 (Fig. 3b). In contrast, the p-mTOR/mTOR ratio was unchanged (Fig. 3c). To confirm that SCH-induced autophagy was initiated by an mTOR-independent mechanism, we assessed the phosphorylation status of an essential component of the ribosome, namely ribosomal protein S6 (rpS6) that is phosphorylated at Ser240/244 following mTOR activation [31]. As shown in Fig. 3d the p-rpS6$^{(Ser240/244)}$/rpS6 ratio was unchanged. Collectively, these data indicate that after SCH, the initiation of autophagy in the RN takes place through an AMPK-dependent pathway.

Accumulation of Autophagosomes in the RN Is Due to Impaired Autophagic Flux

Two types of autophagic dysfunction have been implicated in neurological disorders: (a) impaired initiation of autophagy and (b) defective lysosomal clearance of autophagic substrates due to dysfunctional transport of APs to lysosomes [32]. p62, also called sequestosome 1 (SQSTM1), is an APs cargo protein that targets other proteins that bind to it for selective autophagy. Because p62 accumulates when autophagy is inhibited and because its levels decrease when autophagy is induced, p62 is considered to be a bona fide marker of autophagic activity. Increased levels of p62, associated with greater LC3 conversion, might reflect a reduction in APs degradation due to impairments in autophagic flux [33].

Thus, we determined whether impairments in autophagic flux contribute to the accumulation of LC3-II and APs in rubrospinal neurons after SCH. As indicated in Fig. 4a, starting from day 1 after SCH, p62 levels climbed versus CTRL; this increase became more prominent after 5 days (Fig. 4a), at the peak of accumulation of APs.

To confirm that the accumulation of APs in the rubrospinal neurons after SCH was attributed to impaired autophagic flux, we treated control and SCH rats with the lysosomal inhibitor E64d, which is able to cross the blood–brain barrier (BBB) and efficiently exert its function [34]. Five days after injection, we measured LC3-II/LC3-I ratio and p62 levels by Western

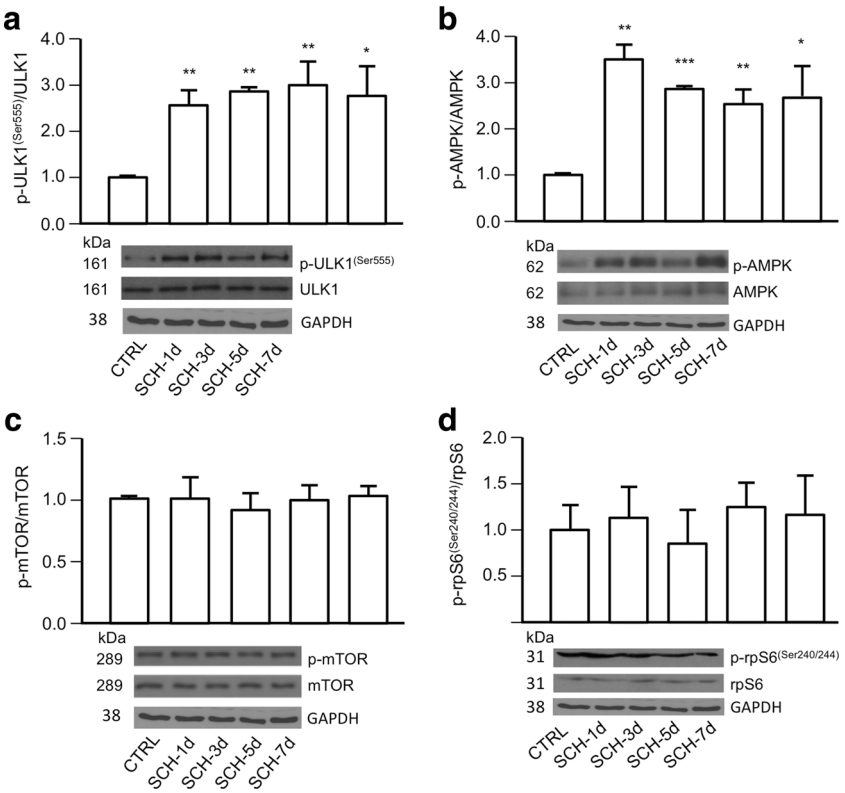

Fig. 3 Autophagy initiation is increased through an AMPK/ULK1-dependent pathway. Representative immunoblotting and densitometry of p-ULK1$^{(Ser555)}$/ULK1 (**a**), p-AMPK/AMPK (**b**), p-mTOR/mTOR (**c**), and p-rpS6$^{(Ser240/244)}$/rpS6 (**d**) expression levels in control (*CTRL*) and lesioned (*SCH*) animals at various time points after injury. Note that starting from 1 day until 5 days after damage (*SCH*), p-ULK1$^{(Ser555)}$/ULK1 and p-AMPK/AMPK levels are increased with respect to *CTRL*. Conversely, no significant changes with respect to *CTRL* are observed in p-mTOR/mTOR and in p-rpS6$^{(Ser240/244)}$/rpS6 levels in *SCH* animals. Data are expressed as mean ± s.d. ($n = 8$/group). One-way ANOVA followed by Bonferroni multiple comparison tests *$p < 0.05$, **$p < 0.01$, ***$p < 0.001$ vs. *CTRL*

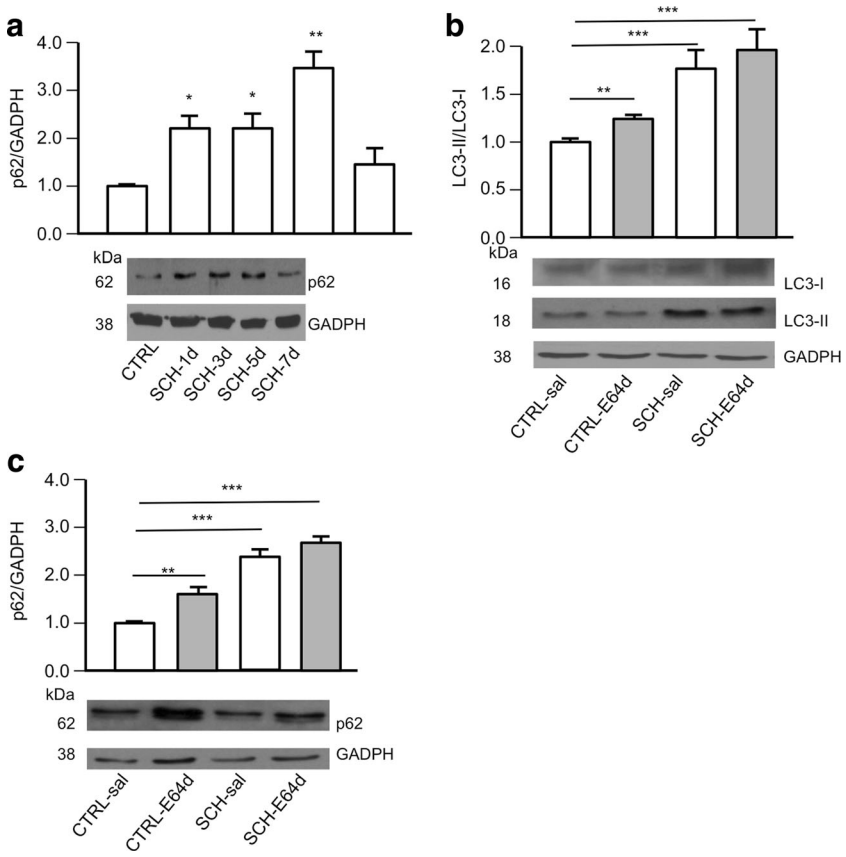

Fig. 4 Autophagy flux and APs clearance are impaired in contralateral red nucleus after SCH. **a** p62 immunoblots and densitometric graphs in control (*CTRL*) and lesioned (*SCH*) animals at various time points. Note that starting from 1 day until 5 days after damage, the downstream marker p62 is increased compared to CTRL. **b**, **c** LC3 and p62 immunoblots and densitometric graphs in control animals treated with saline (*CTRL-sal*) or with E64d (*CTRL-E64d*) and lesioned animals (*SCH*) at 5 days after lesion treated with saline (*SCH-sal*) or E64d (*SCH-E64d*). Note that while treatment with E64d in unlesioned animals (*CTRL*) significantly changes the LC3-II/LC3-I ratio and p62 levels (compare *CTRL-E64d* and *CTRL-sal*), in lesioned animals (*SCH*), it does not (compare *SCH-E64d* and *SCH-sal*). Data are expressed as mean ± s.d. ($n = 8$/group). One-way ANOVA followed by Bonferroni multiple comparison tests. $*p < 0.05$, $**p < 0.01$, $***p < 0.001$ vs. *CTRL*

blot analysis. In control rats, compared with saline treatment, E64d resulted in significantly increase of LC3-II/LC3-I ratio and of p62 levels, as detected by immunoblot analysis (Fig. 4b, c). Conversely, after SCH, E64d did not significantly affect autophagy indices compared to saline treatment (Fig. 4b, c). LC3-II/LC3-I ratio was elevated in the RN from SCH animals versus CTRL, and it did not rise further upon E64d treatment (SCH-sal vs. SCH-E64d; Fig. 4b). Yet, p62 levels in the RN of SCH animals did not increase upon E64d treatment (SCH-sal vs. SCH-E64d; Fig. 4c).

Our data suggest that, after SCH, autophagic flux and APs clearance are impaired in rubrospinal neurons.

Disruption of Autophagic Flux Is Associated with Remote Cell Death

We have demonstrated that rubrospinal degeneration after SCH is associated with mitochondria-dependent apoptosis [35]. To examine the interplay between apoptosis and autophagy in remote damage, we analyzed the kinetics of mitochondria-dependent rubrospinal degeneration and autophagy activation after SCH. Notably, we observed a significant reduction in the soma area of rubrospinal neurons, beginning at 1 day after SCH, compared with the CTRL group (Fig. 5a). Soma area decreased progressively in the subsequent time points, reaching about 72 % of CTRL levels at 5 days, consistent with our previous data [35]. Furthermore, by stereological count, we observe a significant reduction in the total number of rubrospinal neurons, starting from 3 days after injury, reaching about 72 % of CTRL levels at 5 days after SCH (Fig. 5b), as recently reported [35].

Because rubrospinal cell fate after SCH results from mitochondrial dysfunction, we measured the release of cytochrome-C (cyt-c) into the cytosol to identify the molecular events that are associated with rubrospinal degeneration following SCH. By Western blot, cyt-c release increased from 1 day after injury to 5 days (Fig. 5c), with kinetics that were comparable with LC3 as further confirmed by quantitative analysis of densitometric values of LC3 and cyt-c release signals in immunoreacted material (Fig. 5d). Indeed, at 5 days

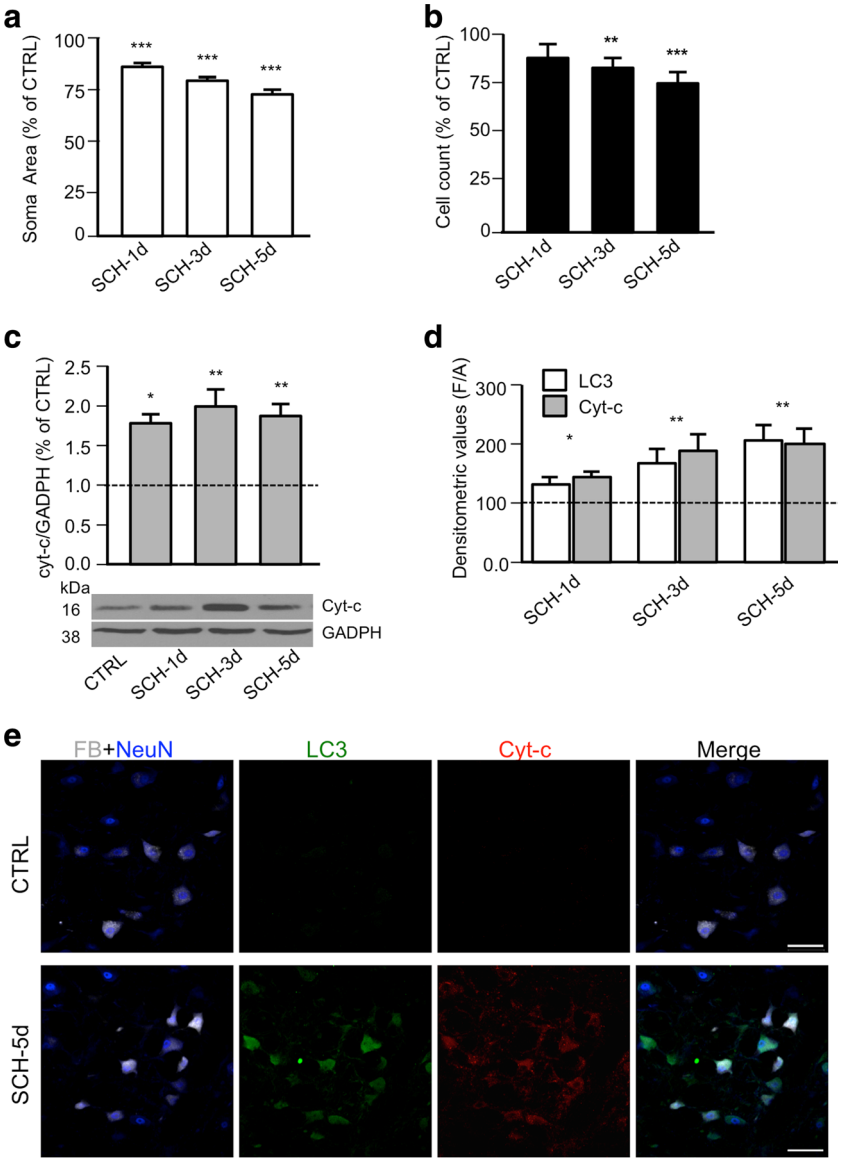

Fig. 5 Disruption of autophagy flux is associated with rubro-spinal degeneration. **a** Histograms of soma area of magnocellular rubrospinal neurons, expressed as percentage of control, in SCH-saline (*SCH-sal*) at various time points after injury. **b** Histograms of stereological counts of FB/Nissl-stained rubrospinal neurons, expressed as percentage of control, in SCH-saline (*SCH-sal*) at various time points after injury. **c** Representative immunoblots and densitometric graphs of time course of cytochrome-c release (*cyt-c*) in red nucleus of CTRL and SCH-saline (*SCH-sal*) at various time points after injury. **d** Histograms of densitometric values of LC3 and cytochrome-c release (*cyt-c*) signals in immunoreacted material, expressed as mean fluorescence of individual cells (*F*) normalized to total cellular surface (**a**) in red nucleus of CTRL and SCH-saline (*SCH*) at various time points after injury (F/A; $n = 250$ cells/group). **e** Triple-labeled and merged confocal images of NeuN (*blue*) plus Fast blue (*FB*; *gray*), LC3 (*green*), and cytochrome-c (*red*) in red nucleus of control (*CTRL*) and 5 days after SCH. Data are expressed as mean ± s.d. ($n = 8$/group). One-way ANOVA followed by Bonferroni multiple comparison tests. $^{*}p < 0.05$, $^{**}p < 0.01$, $^{***}p < 0.001$ vs. CTRL. *Scale bars* = 100 μm

after SCH, most FB-positive rubrospinal neurons strongly co-localized with LC3 and experienced high levels of cyt-c release into the cytosol (Fig. 5e). Thus, impaired autophagic flux correlates with the induction of neuronal apoptosis in the same cells after SCH.

Inhibition of Autophagy Mitigates Remote Neuronal Degeneration After SCH

To determine the effects of autophagic dysfunction in remote regions after SCH, we manipulated autophagy pharmacologically. We stimulated and inhibited APs formation by injecting rapamycin (rapa) and 3-MA, respectively, for 5 days and measured autophagic activity, cyt-c release, neuronal atrophy and survival, and functional recovery in unlesioned (CTRL) and lesioned (SCH) animals. In unlesioned groups, despite differences in pharmacological treatment, no significant changes were observed in autophagic activity, cyt-c release, neuronal atrophy and survival, and functional recovery (Supplementary Fig. 1a–e). In lesioned group, the SCH + rapa animals, although experiencing an increase in APs formation, as demonstrated by LC3 conversion (Fig. 6a), did not differ significantly with regard to cyt-c release (Fig. 6b), neuronal atrophy and death (Fig. 6c, d), and functional recovery (Fig. 6e) compared with SCH + sal animals. In contrast, the SCH + 3-MA group, versus SCH + sal animals, showed reduced APs biogenesis (Fig. 6a), lower cyt-c release (Fig. 6b) and neuronal atrophy (Fig. 6c), greater neuronal survival (Fig. 6d), and better functional recovery (Fig. 6e).

Furthermore, based on the specific involvement of the AMPK pathway in promoting AP formation (Fig. 3b), we selectively inhibited AMPK activity by injecting a single dose of

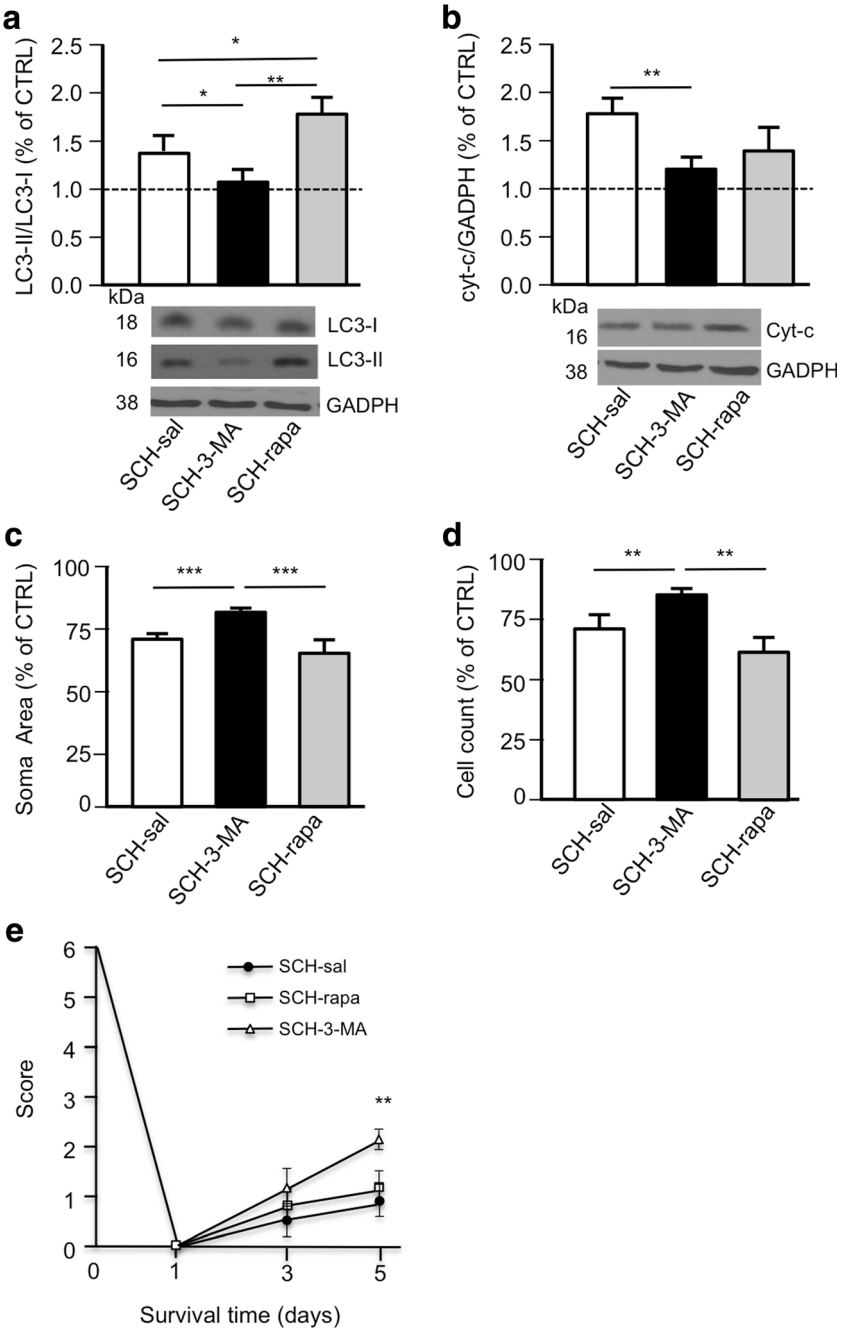

Fig. 6 Inhibition of autophagy reduces degeneration of rubrospinal neurons and improves functional recovery after *SCH*. Representative immunoblots and densitometry of LC3-II/LC3-I ratio (**a**) and cytochrome-c release (**b**) in lesioned animals (*SCH*) treated with saline (*SCH-sal*), 3-methyladenine (*SCH-3-MA*), or rapamycin (*SCH-rapa*) at 5 day after injury. **c** Histograms of soma area of magnocellular rubro-spinal neurons, expressed as percentage of control, in *SCH-sal*, *SCH-3-MA*, or *SCH-rapa* at 5 day after injury. **d** Histograms of stereological counts of FB/Nissl-stained rubrospinal neurons, expressed as percentage of control, in *SCH-sal*, *SCH-3-MA*, and *SCH-rapa* 5 day after injury. **e** Functional recovery evaluation by beam-walk test in *SCH-sal*, *SCH-3-MA*, or *SCH-rapa*. Data are expressed as mean ± s.d. (n = 8/group; n = 10/group for behavior). One-way ANOVA followed by Bonferroni multiple comparison tests $^{*}p < 0.05$, $^{**}p < 0.01$, $^{***}p < 0.001$ vs. *SCH-sal*

compound C (Comp C) i.c.v. 30 min before SCH and measured AP formation, cyt-c release, neuronal atrophy and survival, and functional recovery. Notably, the compound C-dependent decrease in APs biogenesis (Fig. 7a) was associated with a significant reduction in cyt-c release (Fig. 7b), lower neuronal atrophy (Fig. 7c), improved neuronal survival (Fig. 7d), and greater functional recovery (Fig. 7e), consistent with the neurodegenerative effects of autophagy in remote damage after SCH.

These data suggest that APs biogenesis and mitochondria-dependent rubrospinal damage are crucial events early after injury and determine the cellular fate of these neurons.

Discussion

Over the past 5 years, several in vivo studies have shown that various areas of the brain modulate proper basal autophagy on damage to the spinal cord [21, 22, 24, 25]. The role of autophagy in SCI, however, remains debated [18]. In this study, we provide clear evidence that in a model of remote damage after SCI, autophagy is blocked and that enhancement of the APs formation leads neurons to die.

Using a spinal cord hemisection experimental model, we noted early signs of APs formation in damaged rubrospinal

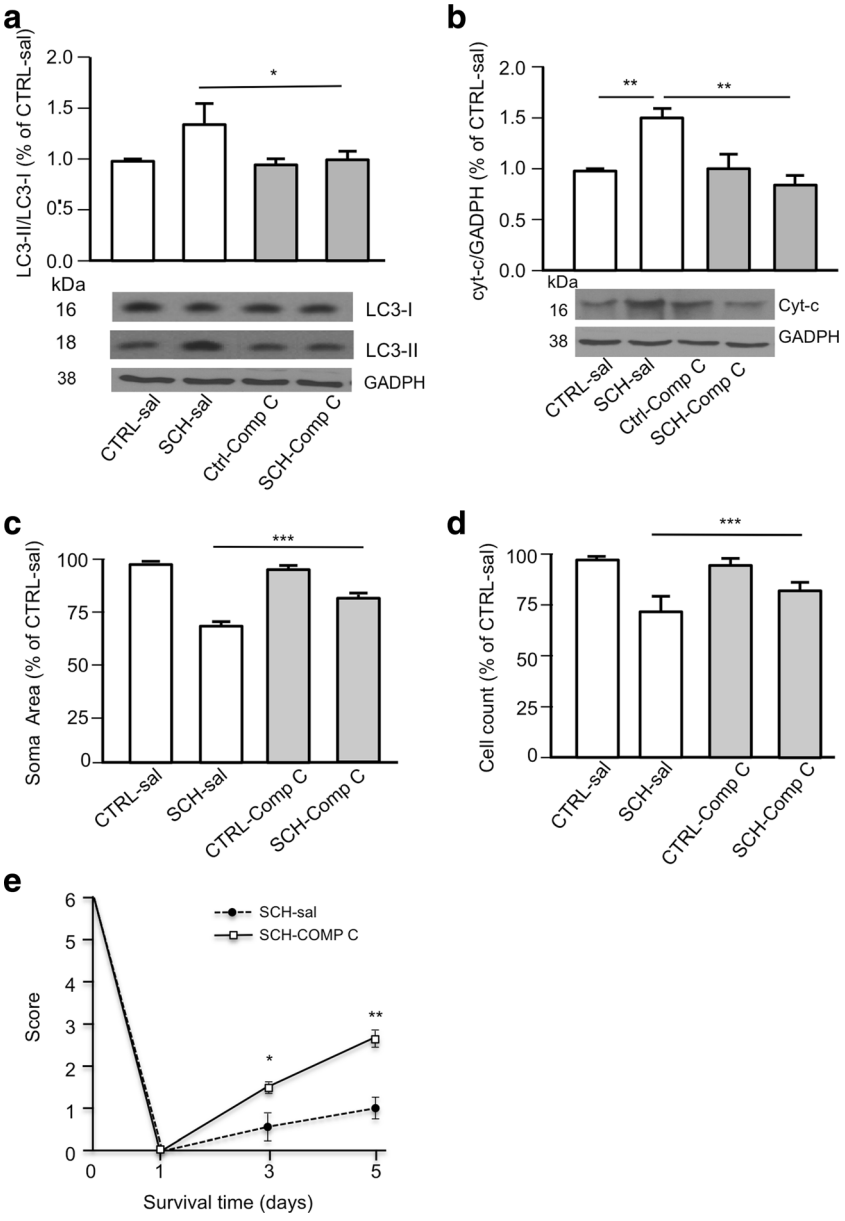

Fig. 7 Autophagy neurotoxic effects are AMPK-dependent. Representative immunoblotting and densitometry of LC3-II/LC3-I (**a**) and cytochrome-c (*cyt-c*) release (**b**) in control (*CTRL*) animals treated with saline (*CTRL-sal*) or compound C (*CTRL-Comp C*) and in lesioned animals (*SCH*) treated with saline (*SCH-sal*) or compound C (*SCH-Comp C*). **c** Histograms of soma sizes of magnocellular rubrospinal neurons, expressed as percentage of *CTRL-sal*, in *CTRL-Comp C*, *SCH-sal*, and *SCH-Comp C* 5 days after injury. **d** Histograms of stereological counts of FB/Nissl-stained rubrospinal neurons, expressed as percentage of *CTRL-sal*, in *CTRL-Comp C*, *SCH-sal*, and *SCH-Comp C* 5 days after injury. **e** Functional recovery evaluation by beam-walk test in lesioned animals (*SCH*) treated with saline (*SCH-sal*) and *Comp C* (*SCH-Comp C*). Data are expressed as mean ± s.d. ($n = 8$/group; $n = 10$/group for behavior). One-way ANOVA followed by Bonferroni multiple comparison tests
$^{*}p < 0.05$, $^{**}p < 0.01$,
$^{***}p < 0.001$

neurons after injury. By morphological analysis, SCH caused the formation of APs in nearly all Fast blue-positive damaged rubrospinal neurons. The peak of APs accumulation, as evidenced by LC3-II levels, occurred early after the lesion, as reported in other SCI experimental models [21, 22, 24].

The APs formation in regions of the brain that are proximal to damage has been described [21, 22, 24]. In our study, we provide novel evidence that SCI elicits a robust APs accumulation in distal regions, such as the red nucleus. Notably, APs accumulated exclusively in neurons, not in astrocytes, activated microglia, or oligodendrocytes as reported [21, 24, 36, 37].

Impairments in autophagic flux have been reported in neurodegenerative diseases and have been proposed to contribute to the pathological accumulation of APs, neuronal dysfunction, and death after SCI and TBI [18, 24, 38]. We observed the pronounced accumulation of autophagy substrates, such as SQSTM1/p62. SQSTM1/p62 acts as a link between LC3 and ubiquitinated substrates and is efficiently degraded by autophagy [39]. In combination with other parameters, such as LC3-II turnover, SQSTM1/p62 is considered to be a reliable marker for studying autophagic flux [27]. The impairment in autophagic flux was confirmed by observations that E64d, a lysosomal inhibitor that can penetrate the BBB [34], did not increase LC3-II/LC3-I ratio further. This result is notable, because in another model of remote degeneration, based on cerebellar lesions, we demonstrated that the

accumulation of APs was independent on the block in autophagic flux [19]. The reasons for these differences between studies are unknown. It is possible that various injury models or severities of injury differentially affect autophagic activation and the ability of autophagic flux to be completed [18].

Our findings clearly show that pharmacological stimulation of APs biogenesis by rapamycin failed to halt mitochondrial damage, atrophy, and the death of rubrospinal neurons, demonstrating that pro-autophagy treatments, during blockade of autophagic flux, are ineffective or even detrimental [40]. Conversely, inhibition of APs formation by 3-MA significantly reduced cytochrome-c release from damaged mitochondria and mitigated atrophy and death in rubrospinal neurons, confirming that impairments in autophagic flux after SCH contribute to the induction and enhancement of apoptotic cell death in these neurons.

Taken together, our results prove that SCH causes the accumulation of dysfunctional APs limiting their clearance. The impairment in APs degradation may lead to the accumulation of neurotoxic proteins and the ensuing neuronal cell death. In fact, the beneficial effect of 3-MA and compound C is to slowdown the formation of dysfunctional APs rather than limit the entire autophagy activity. Similarly, the detrimental effect of rapamycin may be due to the accumulation of APs, which cannot be degraded, causing neuronal death.

These findings are consistent with previous studies on another model of axonal damage that involves the optic nerve, which reported that local application of 3-MA significantly delayed axonal degeneration following a nerve lesion [41]. Furthermore, considering that the initiation of autophagy in our model depends on AMPK activity, its inhibition confirms the deleterious effects of autophagy in remote neurons after SCH.

Our study has several limitations. We used an autophagy inhibitor, 3-MA, to determine whether autophagy contribute to remote degeneration after SCI. 3-MA has several effects that are independent on its inhibition of autophagy, influencing cellular function and signaling [42, 43]. However, the results obtained with rapamycin and compound C treatments suggest that the effect of 3-MA is due to its ability to inhibit APs biogenesis.

Our novel work contributes to the pathophysiological profile of SCI, indicating that autophagy is an executive step that is involved in neuronal degeneration at various levels. Furthermore, our data reveal a potential common mechanism that mediates secondary damage after SCI and support that strategies aimed at targeting autophagy should be considered in the development of new therapeutic approaches against traumatic brain and spinal cord injuries.

Acknowledgments This work was supported by the International Research for Paraplegia (P141 to M.T.V.) and by the Italian Ministry of Health (Ricerca Corrente; to M. M.) and partially by the program Young Researchers of Italian Ministry of Health (GR-2010.2310524 to M.T.V.; GR-2011-02351457 to M.D.). The professional editorial work of Blue Pencil Science is also acknowledged.

Compliance with Ethical Standard

Conflict of Interest The authors declare that they have no conflict of interest.

References

1. Kwon BK, Tetzlaff W, Grauer JN, Beiner J, Vaccaro AR (2004) Pathophysiology and pharmacologic treatment of acute spinal cord injury. Spine J 4(4):451–464. doi:10.1016/j.spinee.2003.07.007
2. Cadotte DW, Fehlings MG (2011) Spinal cord injury: a systematic review of current treatment options. Clin Orthop Relat Res 469(3): 732–741. doi:10.1007/s11999-010-1674-0
3. Wu B, Ren X (2009) Promoting axonal myelination for improving neurological recovery in spinal cord injury. J Neurotrauma 26(10): 1847–1856. doi:10.1089/neu.2008.0551
4. Bradbury EJ, Carter LM (2011) Manipulating the glial scar: chondroitinase ABC as a therapy for spinal cord injury. Brain Res Bull 84(4–5):306–316. doi:10.1016/j.brainresbull.2010.06.015
5. Bonner JF, Steward O (2015) Repair of spinal cord injury with neuronal relays: from fetal grafts to neural stem cells. Brain Res 1619:115–123. doi:10.1016/j.brainres.2015.01.006
6. Ramer LM, Ramer MS, Bradbury EJ (2014) Restoring function after spinal cord injury: towards clinical translation of experimental strategies. The Lancet Neurology 13(12):1241–1256. doi:10.1016/S1474-4422(14)70144-9
7. Viscomi MT, Molinari M (2014) Remote neurodegeneration: multiple actors for one play. Mol Neurobiol 50(2):368–389. doi:10.1007/s12035-013-8629-x
8. Block F, Dihne M, Loos M (2005) Inflammation in areas of remote changes following focal brain lesion. Prog Neurobiol 75(5):342–365. doi:10.1016/j.pneurobio.2005.03.004
9. Klionsky DJ (2005) The molecular machinery of autophagy: unanswered questions. J Cell Sci 118(Pt 1):7–18. doi:10.1242/jcs.01620
10. Levine B, Klionsky DJ (2004) Development by self-digestion: molecular mechanisms and biological functions of autophagy. Dev Cell 6(4):463–477
11. Mizushima N (2007) Autophagy: process and function. Genes Dev 21(22):2861–2873. doi:10.1101/gad.1599207
12. Rubinsztein DC, DiFiglia M, Heintz N, Nixon RA, Qin ZH, Ravikumar B, Stefanis L, Tolkovsky A (2005) Autophagy and its possible roles in nervous system diseases, damage and repair. Autophagy 1(1):11–22
13. Nixon RA (2013) The role of autophagy in neurodegenerative disease. Nat Med 19(8):983–997. doi:10.1038/nm.3232
14. Sarkar S (2013) Regulation of autophagy by mTOR-dependent and mTOR-independent pathways: autophagy dysfunction in neurodegenerative diseases and therapeutic application of autophagy enhancers. Biochem Soc Trans 41(5):1103–1130. doi:10.1042/BST20130134
15. Nixon RA, Wegiel J, Kumar A, Yu WH, Peterhoff C, Cataldo A, Cuervo AM (2005) Extensive involvement of autophagy in Alzheimer disease: an immuno-electron microscopy study. J Neuropathol Exp Neurol 64(2):113–122

16. Nixon RA, Yang DS (2011) Autophagy failure in Alzheimer's disease—locating the primary defect. Neurobiol Dis 43(1):38–45. doi:10.1016/j.nbd.2011.01.021
17. Rubinsztein DC (2006) The roles of intracellular protein-degradation pathways in neurodegeneration. Nature 443(7113): 780–786. doi:10.1038/nature05291
18. Lipinski MM, Wu J, Faden AI, Sarkar C (2015) Function and mechanisms of autophagy in brain and spinal cord trauma. Antioxid Redox Signal 23(6):565–577. doi:10.1089/ars.2015.6306
19. Viscomi MT, D'Amelio M, Cavallucci V, Latini L, Bisicchia E, Nazio F, Fanelli F, Maccarrone M, Moreno S, Cecconi F, Molinari M (2012) Stimulation of autophagy by rapamycin protects neurons from remote degeneration after acute focal brain damage. Autophagy 8(2):222–235. doi:10.4161/auto.8.2.18599
20. Cavallucci V, Bisicchia E, Cencioni MT, Ferri A, Latini L, Nobili A, Biamonte F, Nazio F, Fanelli F, Moreno S, Molinari M, Viscomi MT, D'Amelio M (2014) Acute focal brain damage alters mitochondrial dynamics and autophagy in axotomized neurons. Cell Death Dis 5:e1545. doi:10.1038/cddis.2014.511
21. Kanno H, Ozawa H, Sekiguchi A, Itoi E (2009) Spinal cord injury induces upregulation of Beclin 1 and promotes autophagic cell death. Neurobiol Dis 33(2):143–148. doi:10.1016/j.nbd.2008.09.009
22. Kanno H, Ozawa H, Sekiguchi A, Yamaya S, Itoi E (2011) Induction of autophagy and autophagic cell death in damaged neural tissue after acute spinal cord injury in mice. Spine 36(22): E1427–E1434. doi:10.1097/BRS.0b013e3182028c3a
23. Tang P, Hou H, Zhang L, Lan X, Mao Z, Liu D, He C, Du H, Zhang L (2014) Autophagy reduces neuronal damage and promotes locomotor recovery via inhibition of apoptosis after spinal cord injury in rats. Mol Neurobiol 49(1):276–287. doi:10.1007/s12035-013-8518-3
24. Liu S, Sarkar C, Dinizo M, Faden AI, Koh EY, Lipinski MM, Wu J (2015) Disrupted autophagy after spinal cord injury is associated with ER stress and neuronal cell death. Cell Death Dis 6:e1582. doi:10.1038/cddis.2014.527
25. Ribas VT, Schnepf B, Challagundla M, Koch JC, Bahr M, Lingor P (2015) Early and sustained activation of autophagy in degenerating axons after spinal cord injury. Brain Pathol 25(2):157–170. doi:10.1111/bpa.12170
26. Klionsky DJ, Abdalla FC, Abeliovich H, et al. (2012) Guidelines for the use and interpretation of assays for monitoring autophagy. Autophagy 8(4):445–544
27. Klionsky DJ, Abdelmohsen K, Abe A, et al. (2016) Guidelines for the use and interpretation of assays for monitoring autophagy (3rd edition). Autophagy 12(1):1–222. doi:10.1080/15548627.2015.1100356
28. Chan EY, Kir S, Tooze SA (2007) siRNA screening of the kinome identifies ULK1 as a multidomain modulator of autophagy. J Biol Chem 282(35):25464–25474. doi:10.1074/jbc.M703663200
29. Egan D, Kim J, Shaw RJ, Guan KL (2011) The autophagy initiating kinase ULK1 is regulated via opposing phosphorylation by AMPK and mTOR. Autophagy 7(6):643–644
30. Kim J, Kundu M, Viollet B, Guan KL (2011) AMPK and mTOR regulate autophagy through direct phosphorylation of Ulk1. Nat Cell Biol 13(2):132–141. doi:10.1038/ncb2152
31. Jung CH, Ro SH, Cao J, Otto NM, Kim DH (2010) mTOR regulation of autophagy. FEBS Lett 584(7):1287–1295. doi:10.1016/j.febslet.2010.01.017
32. Levine B, Kroemer G (2008) Autophagy in the pathogenesis of disease. Cell 132(1):27–42. doi:10.1016/j.cell.2007.12.018
33. Zhang R, Zhang LH, Xie X (2013) iPSCs and small molecules: a reciprocal effort towards better approaches for drug discovery. Acta Pharmacol Sin 34(6):765–776. doi:10.1038/aps.2013.21
34. Tsubokawa T, Yamaguchi-Okada M, Calvert JW, Solaroglu I, Shimamura N, Yata K, Zhang JH (2006) Neurovascular and neuronal protection by E64d after focal cerebral ischemia in rats. J Neurosci Res 84(4):832–840. doi:10.1002/jnr.20977
35. Latini L, Bisicchia E, Sasso V, Chiurchiu V, Cavallucci V, Molinari M, Maccarrone M, Viscomi MT (2014) Cannabinoid CB2 receptor (CB2R) stimulation delays rubrospinal mitochondrial-dependent degeneration and improves functional recovery after spinal cord hemisection by ERK1/2 inactivation. Cell Death Dis 5:e1404. doi:10.1038/cddis.2014.364
36. Chen HC, Fong TH, Lee AW, Chiu WT (2012) Autophagy is activated in injured neurons and inhibited by methylprednisolone after experimental spinal cord injury. Spine 37(6):470–475. doi:10.1097/BRS.0b013e318221e859
37. Hao HH, Wang L, Guo ZJ, Bai L, Zhang RP, Shuang WB, Jia YJ, Wang J, Li XY, Liu Q (2013) Valproic acid reduces autophagy and promotes functional recovery after spinal cord injury in rats. Neurosci Bull 29(4):484–492. doi:10.1007/s12264-013-1355-6
38. Sarkar C, Zhao Z, Aungst S, Sabirzhanov B, Faden AI, Lipinski MM (2014) Impaired autophagy flux is associated with neuronal cell death after traumatic brain injury. Autophagy 10(12):2208–2222. doi:10.4161/15548627.2014.981787
39. Bjorkoy G, Lamark T, Brech A, Outzen H, Perander M, Overvatn A, Stenmark H, Johansen T (2005) p62/SQSTM1 forms protein aggregates degraded by autophagy and has a protective effect on huntingtin-induced cell death. J Cell Biol 171(4):603–614. doi:10.1083/jcb.200507002
40. Lipinski MM, Zheng B, Lu T, Yan Z, Py BF, Ng A, Xavier RJ, Li C, Yankner BA, Scherzer CR, Yuan J (2010) Genome-wide analysis reveals mechanisms modulating autophagy in normal brain aging and in Alzheimer's disease. Proc Natl Acad Sci U S A 107(32): 14164–14169. doi:10.1073/pnas.1009485107
41. Knoferle J, Koch JC, Ostendorf T, Michel U, Planchamp V, Vutova P, Tonges L, Stadelmann C, Bruck W, Bahr M, Lingor P (2010) Mechanisms of acute axonal degeneration in the optic nerve in vivo. Proc Natl Acad Sci U S A 107(13):6064–6069. doi:10.1073/pnas.0909794107
42. Heckmann BL, Yang X, Zhang X, Liu J (2013) The autophagic inhibitor 3-methyladenine potently stimulates PKA-dependent lipolysis in adipocytes. Br J Pharmacol 168(1):163–171. doi:10.1111/j.1476-5381.2012.02110.x
43. Marinelli S, Nazio F, Tinari A, Ciarlo L, D'Amelio M, Pieroni L, Vacca V, Urbani A, Cecconi F, Malorni W, Pavone F (2014) The autophagic inhibitor 3-methyladenine potently stimulates PKA-dependent lipolysis in adipocytes. Pain 155(1):93–107. doi:10.1016/j.pain.2013.09.013